

Simulated neutrino signals of low and intermediate energy neutrinos on Cd detectors

J. Sinatkas*

Department of Informatics Engineering, Technological Institute of Western Macedonia, Kastoria, GR-52100

V. Tsakstara†

*Electrical Engineering Department, Technological Institute of Western Macedonia,
School of Applied Science, Kozani, GR-50100 and
Division of Theoretical Physics, University of Ioannina, GR-45110 Ioannina, Greece*

Odysseas Kosmas‡

Modelling and Simulation Centre, MACE, University of Manchester, Sackville Street, Manchester, UK

(Dated: April 3, 2019)

Neutrino-nucleus reactions cross sections, obtained for neutrino energies in the range $\varepsilon_\nu \leq 100 - 120$ MeV (low- and intermediate-energy range), which refer to promising neutrino detection targets of current terrestrial neutrino experiments, are presented and discussed. At first, we evaluated original cross sections for elastic scattering of neutrinos produced from various astrophysical and laboratory neutrino sources with the most abundant Cd isotopes ^{112}Cd , ^{114}Cd and ^{116}Cd . These isotopes constitute the main material of the COBRA detector aiming to search for neutrinoless double beta decay events and neutrino-nucleus scattering events at the Gran Sasso laboratory (LNGS). The coherent ν -nucleus reaction channel addressed with emphasis here, dominates the neutral current ν -nucleus scattering, events of which have only recently been observed for a first time in the COHERENT experiment at Oak Ridge. Subsequently, simulated ν -signals expected to be recorded at Cd detectors are derived through the application of modern simulation techniques and employment of reliable neutrino distributions of astrophysical ν -sources (as the solar, supernova and Earth neutrinos), as well as laboratory neutrinos (like the reactor neutrinos, the neutrinos produced from pion-muon decay at rest and the β -beam neutrinos produced from the acceleration of radioactive isotopes at storage rings as e.g. at CERN).

PACS numbers: 26.50.+x, 25.30.Pt, 97.60.Bw, 25.30.-c, 23.40.Bw, 21.60.Jz

Keywords: Nuclear detector responses, neutrino nucleus cross sections, supernova neutrino detection, neutral-current neutrino-nucleus processes, quasi-particle random phase approximation

I. INTRODUCTION

In recent interdisciplinary investigations in nuclear, particle and astro-particle physics, the interactions of neutrinos with matter play key role in understanding deeply the underlying physics. Exact measurements and reliable models of neutrino-matter interactions provide unquestionable requirements for unravelling top physics issues as neutrino properties, neutrino oscillations, supernova dynamics, dark matter detection and many others [1–4]. To enable further progress, relevant nuclear model calculations, across a wide energy range and in various nuclear isotopes, may provide significant results [5–7].

Recently, the neutrino-nucleon and neutrino-nucleus cross-section uncertainties have reached a limiting factor in the judgement of neutrino interaction models and in interpreting many neutrino experiments [1–4] and specifically experiments like the COHERENT where recently coherent neutrino nucleus scattering events have been measured for a first time [8–10]. Furthermore, the presence of important nuclear effects impact the interaction cross sections as well as the final nuclear states reached through the scattering process [11–13]. The nuclear effects also affect the rebuilding of the incoming ν -energy spectra of the neutrino sources that are key-role input for the resolution of neutrino detection signals. Understanding neutrino-nucleus scattering processes provides to experimentalists good information to separate the background events from the detection signal [14–20].

The current neutrino physics searches are categorized according to the incident neutrino energy in the scattering process. Thus, the range below about 10 MeV (low-

*Electronic address: sinatkas@kastoria.teiwm.gr

†Electronic address: vtsaksta@cc.uoi.gr

‡Electronic address: odysseas.kosmas@manchester.ac.uk

energy, from a nuclear physics viewpoint) is connected to Geo-neutrino and solar neutrino studies [14–19], the neutrino energy range of 10 up to about 100–120 MeV (intermediate energy) covers a set of ν -physics topics in the front of nuclear structure physics and astro-particle physics such as core-collapse supernovae dynamics and dark matter detection [11–13, 21, 22], while the energy range from 0.1–0.2 GeV up to about 10 GeV is related to meson decay neutrino beams such as those employed for long-baseline (high energy) neutrino experiments [23–26].

Due to the fact that neutrinos interact very weakly, they are unique messengers from astrophysical sources (the Earth, the Sun, the supernovae and other stars) [1, 2, 21] allowing us to investigate deep into the astrophysical objects [21, 27–29]. In the near future, remarkably sensitive detectors as liquid-scintillator detectors, liquid argon time projection chambers and water-Cherenkov detectors would operate aiming to study neutrino physics issues of astrophysical neutrino sources [19, 20, 26] (for higher energy neutrinos, like e.g. those coming from active galactic nuclei, black hole binary stars, etc. operating detectors as IceCube, KM3Net and others are appropriate) [30, 31]. Each detector type has specific advantages (e.g. for supernova neutrinos, a combination of all types may allow for a better investigation of the relevant open issues).

Our present work focuses on the interpretation of various ν signals generated in nuclear detectors of terrestrial neutrino experiments through the investigation of the nuclear response of Cd detector materials to various neutrino energy spectra [3, 4, 26, 32]. We emphasize on signals coming from geo-neutrinos, solar-neutrinos, supernova-neutrinos, reactor-neutrinos and neutrinos generated from the decay of stopped pions and muons.

The main ingredients to this aim are: (i) The original differential and integrated cross sections of the neutral-current reactions of neutrinos, $^{112,114,116}\text{Cd}(\nu, \nu')^{112,114,116}\text{Cd}^*$, and anti-neutrinos, $^{112,114,116}\text{Cd}(\bar{\nu}, \bar{\nu}')^{112,114,116}\text{Cd}^*$, computed for the coherent channel by using a refinement of the quasi particle random phase approximation (QRPA) [11, 13, 32–34]. (ii) Reliable descriptions of the shapes of neutrino energy distributions coming out of numerical simulations of distributions in neutrino-energies $\varepsilon_\nu \leq 100 - 120$ MeV (for the above mentioned ν -sources). (iii) Modern computational tools [35–39] for the required folding (convolution) procedure in order to simulate the signal expected to be recorded on the Cd detectors CdTe or CdZnTe (the detector media of COBRA experiment) [3, 4, 26] from neutrino sources as the geo-, reactor-, solar-, supernova- and pion/muon decay neutrinos. We mention that, the response of the Cd isotopes in the particle-bound excitation region, which coincides with the energy range of geo-neutrinos, is rather rich and this is one of the motivations for performing the present calculations. The next generation detectors (LENA, Borexino, SNO+) [19, 20], are expected to give useful answers to several questions of

geological importance regarding the precise geo- ν fluxes and abundances of natural radioactive elements (K , U , Th) in the Earth’s interior [40–43].

In this work we pay special attention on the coherent elastic neutrino-nucleus scattering (CEvNS) that is a process in which the target nucleus recoils coherently via a combined neutral current exchange width with neutrinos or anti-neutrinos. This process is well predicted by the standard model of the electroweak interactions and has large cross sections (10^{-39} cm^2 in the neutrino-energy region ($\varepsilon_\nu \leq 50$ MeV)). This process has very recently been observed in the COHERENT experiment at a 6.7σ confidence level (CL), by using a low-background CsI[Na] scintillator [8–10]. The detector was exposed to a ν_μ neutrino beam coming from the Spallation Neutron Source (SNS) at Oak Ridge, USA [9]. This facility generates the most intense (pulsed) neutron beam in the world while simultaneously a significant yield of neutrinos is generated when pions (product of proton interactions in the target) decay at rest (prompt neutrinos). In addition, the muons produced from the charged-pion decay generate the known as delayed neutrino beam [10].

Even though many groups world-wide are now studying the difficult low-energy nuclear recoil signature, only a few sources, in specific nuclear reactors and spallation neutron sources yield the required neutrino-energy beams in adequate quantities for such measurements [44–46]. In our present theoretical work, we do not address the improved constraints derived from this dataset on non-standard neutrino interactions with quarks (for a comprehensive discussion on this issue the reader is referred e.g. to Refs. [47, 48] and references therein). The present article is an extension of our previous calculations performed in Ref. [11, 13, 32] and we used the same but slightly improved nuclear method. The extension refers to the employment of new detector isotopes and the better accuracy of the calculations [11–13, 32].

In the rest of the paper, at first (Sections 2 and 3), the main formalism is described and original cross sections calculations are presented. Then (Sections 4 and 5), a description of the main characteristics of the low and intermediate energy neutrino sources addressed here are briefly summarized and folded cross sections as well as event rates for neutral current neutrino scattering off the ^{112}Cd , ^{114}Cd and ^{116}Cd isotopes are presented and discussed. Finally (Section 6), the main conclusions of the present work are extracted.

II. BRIEF DESCRIPTION OF THE FORMALISM

A. Angle differential coherent ν -nucleus cross section

In the description of the ν -nucleus scattering, the angle differential cross section $d\sigma/d\Omega$ is a useful quantity. For the elastic-scattering of a neutrino with energy ε_ν on a

nucleus (A,Z) the angle differential cross section (with respect to the the scattering angle ϑ) is defined as [47, 49–51]

$$\frac{d\sigma}{d\Omega} = \frac{G_F^2}{4\pi^2} \varepsilon_\nu^2 (1 + \cos \vartheta) \frac{Q_w^2}{4} \mathcal{F}(q^2)^2 \quad (1)$$

($G_F = 1.1664 \times 10^{-5}$ GeV $^{-2}$ is the Fermi weak coupling constant). In this definition, the quantity $\mathcal{F}(q^2)$ includes the nuclear structure dependence of the cross section as [33, 34]

$$\mathcal{F}(q^2) = \frac{1}{Q_w} \left[(1 - 4 \sin^2 \Theta_w) Z F_Z(q^2) - N F_N(q^2) \right] \quad (2)$$

where Θ_w denotes the weak mixing angle, known as Weinberg angle which takes the value $\sin^2 \Theta_w \approx 0.2313$. In Eqs. (1) and (2), Q_w denotes the weak charge of the target nucleus given by

$$Q_w = (1 - 4 \sin^2 \Theta_w) Z - N. \quad (3)$$

The latter expression shows that, the neutron coherence of neutral currents (NC), in the case of neutron rich targets, provides large cross sections. This effect can be exploited in detecting, e.g. earth and sky neutrinos by measuring nuclear recoils. Measurements of these (NC) cross sections may also provide useful information about the neutrino source [21] and yield information about the primary neutrino fluxes, i.e. before flavour conversions in the neutrino sphere of core collapse supernovae.

The sensitivity of the coherent scattering channel to the neutron number in the target nucleus, may provide nuclear structure information through investigation of ν -nucleus scattering and the possibility to search for non-standard neutrino physics by taking advantage of the flavour-blind nature of the process [48, 52].

The ground-state elastic nuclear form factors, $F_Z(q^2)$ for protons and $F_N(q^2)$ for neutrons entering Eq. (2), are defined by

$$F_k(q^2) = \frac{k}{4\pi} \int j_0(qr) \rho_{n,p}(r) r^2 dr, \quad k = N, Z \quad (4)$$

and are normalized as $F_{N,Z}(q^2 = 0) = 1$. In the latter equation, $\rho_{n,p}(r)$ denote the neutron (n) and proton (p) charge density distributions with $j_0(qr) = \sin(qr)/(qr)$ being the zero-order spherical Bessel function (we neglect a small correction from the single-nucleon form factors proportional to $e^{-(qb_N)^2/6}$ with $b_N \approx 0.8$ fm being the nucleon harmonic oscillator size parameter [53]). The proton density $\rho_p(r)$ is often taken from experiment whenever measured charge densities are available [33, 49].

Moreover, assuming that $F_N \approx F_Z$, from Eqs. (1) and (2) (in nuclei with $J^\pi = 0^+$ ground state), one obtains

$$\frac{d\sigma(\varepsilon_\nu, \vartheta)}{d\cos\vartheta} = \frac{G_F^2}{2\pi} (1 + \cos \vartheta) \varepsilon_\nu^2 \left[f_V^p Z + f_V^n N \right]^2 F_Z^2(q^2). \quad (5)$$

where f_V^p and f_V^n stand for the polar-vector couplings of the weak neutral current

$$f_V^p = \frac{1}{2} - 2 \sin^2 \Theta_w, \quad f_V^n = -\frac{1}{2}. \quad (6)$$

Thus, the coherent cross section depends on the square of the ground-state nuclear form factor $\mathcal{F}(q^2)$ at momentum transfer q given by

$$q = 2\varepsilon_\nu \sin(\vartheta/2), \quad (7)$$

From Eq. (2), we see that, since $f_V^p = (1 - 4 \sin^2 \Theta_w)/2 \approx 0.0374$ is small, a neutrino scattered elastically on a spin-zero nucleus couples mostly to the neutron distribution, $\rho_n(r)$. A measurement of the cross section for this process would, at some level, provide a determination of the neutron form factor $F_N(q^2)$ [52, 54]. Some authors consider that this would be complementary to parity violating experiments [50, 52] because it would provide additional data, obtained at different energy ranges and with different nuclei that could be used to calibrate nuclear structure calculations [33, 34, 49–51].

In earlier astrophysical estimations of the coherent scattering cross sections within the Standard Model (SM) [51, 55] (also in recent beyond the SM calculations [56, 57]), the approximation $F_N(q^2) \approx F_Z(q^2) \approx 1$ was used for the total coherent cross section $\sigma_{tot}(\varepsilon_\nu)$ written as

$$\sigma_{tot}(\varepsilon_\nu) = \frac{G_F^2}{8\pi} \left[(1 - 4 \sin^2 \Theta_w) Z - N \right]^2 \varepsilon_\nu^2. \quad (8)$$

(we mention that available experimental data for neutron form factors are very limited).

From an experimental point of view, and particularly for the neutrino facilities near spallation sources [45, 58], it is also interesting the expression of the coherent differential cross section as a function of the nuclear recoil energy T_A . This is approximately written as [58–61]

$$\frac{d\sigma(\varepsilon_\nu, T_A)}{dT_A} = \frac{G_F^2}{4\pi} Q_w^2 M \left(1 - \frac{MT_A}{2\varepsilon_\nu^2} \right) F(2MT_A^2), \quad (9)$$

where M is the nuclear mass and F denotes the ground state elastic form factor of the target nucleus. For the sake of completeness, we note that other expressions, including higher order terms with respect to T_A can be found, see e.g. Refs. [9, 10, 58–60]. The contribution, however, of these terms is negligible and thus, higher order terms in Eq. (9) does not influence essentially the calculations. Our present coherent differential cross sections are not obtained as functions of the recoil energy but as functions of the scattering angle or the momentum transfer connected through Eq. (7).

It should be noted that, the signal on the coherent neutrino-nucleus scattering experiments is significantly different compared to that of the incoherent scattering where the signal could be an outgoing particle or a de-excitation product [32].

The total coherent cross section $\sigma_{tot}(\varepsilon_\nu)$ is obtained by integrating numerically Eq. (5) over the angle θ ($\theta_{min} = 0$ to $\theta_{max} = \pi$) or Eq. (9) over T_A between

$$T_A^{min} = \frac{T_A}{2} + \sqrt{\frac{T_A}{2}(M_A + \frac{T_A}{2})},$$

to $T_A^{max} = \infty$ [47, 61, 62].

Before closing this sections, it is worth mentioning that, in our present calculations of the neutrino-nucleus cross sections part of the cross-section uncertainties are removed by performing realistic nuclear structure calculations for both proton and neutron nuclear form factors (for a recent comprehensive discussion on this issue the reader is referred e.g. to Ref. [48] where the results coming out of different nuclear models and various approximations are presented and discussed).

III. ORIGINAL CROSS SECTION CALCULATIONS

The neutral-current scattering of low and intermediate energy neutrinos ν_ℓ or anti-neutrinos $\tilde{\nu}_\ell$ ($\ell = e, \mu, \tau$) off the $^{112,114,116}\text{Cd}$ isotopes (with abundances 24.13%, 28.8% and 7.5%, respectively, the first two are the most abundant Cd isotopes) are represented by

$$\nu_l(\tilde{\nu}_l) + {}^{112,114,116}\text{Cd} \rightarrow {}^{112,114,116}\text{Cd}^* + \nu'_l(\tilde{\nu}'_l), \quad (10)$$

(Cd* denote excited states of Cd-isotopes). We mention that, the above reactions of the Cd-isotopes and also the charged-current (CC) reactions for $\ell = e$, play significant role in astrophysical environment by affecting the electron fraction Y_e of the matter and its strong effect on the matter flow [22, 63–66].

In the first step of the present calculations, we evaluate original cross sections for the coherent channel (ground state to ground state transitions) of the reactions of Eq. (10) [5, 11, 13, 62, 67, 68]. As can be seen from Eq. (5), the original cross section for scattering of neutrinos, ν_l or anti-neutrinos, $\tilde{\nu}_l$, are identical (this holds only for the coherent channel). The signal (folded cross section) on the nuclear detector, however, as we will see in Sections IV and V, could be significantly different. This is due to the flavour dependent energy distributions of the ν -beam reaching the nuclear detector, that enters in the folding procedure.

In this work, the required nuclear ground state wave functions are obtained from mean-field calculations using the successful Woods-Saxon interaction plus the monopole (pairing) interaction of the Bonn C-D potential. The ground state of the studied (even-even) $^{112,114,116}\text{Cd}$ isotopes (they have ground state spin $|J_i^{\pi_i}\rangle = |0_{gs}^+\rangle$) is computed by solving iteratively the BCS equations [11, 13, 32, 47, 69].

In Table I, we list the values of the resulting pairing parameters ($g_{pair}^{p,n}$) and the (theoretical) energy gaps ($\Delta_{p,n}^{th}$) for protons (p) and neutrons (n) determined at

the BCS level for the above isotopes. As is well known, these parameters renormalise the pairing interaction of the Bonn C-D potential in order to fit the theoretical gaps, $\Delta_{p,n}^{th}$, to the empirical ones $\Delta_{p,n}^{exp}$. The latter are provided through the application of the three point formulas (see Appendix) by using the empirical separation energies (for protons and neutrons, $S_{p,n}$) of the neighbouring nuclear isotopes [13, 32]. The values of the $g_{pair}^{p,n}$ adjust reliably the empirical energy gaps (see Table I) [11, 13, 32, 69, 70].

The needed proton and neutron nuclear form factors in the context of QRPA are calculated from the expressions

$$F_k(q^2) = \frac{1}{k} \sum_j \hat{j} \langle (n\ell)j | j_0(qr) | (n\ell)j \rangle (V_j^k)^2, \quad k = N, Z \quad (11)$$

(V_j^k denotes the probability amplitude for proton or neutron occupancies of the single particle $(n\ell)j$ -level). The summation, runs over the 15 active levels of the chosen model space (the same for proton and neutrons) as well as over the fully occupied j -levels for which $V_j^k = 1$ (they describe a ^{40}Ca closed core). The model space assumed consists of the major harmonic oscillator shells having quantum numbers $N=3, 4, 5$ ($N=2n + \ell$).

In Fig. 1, the quantities needed for calculating the differential and integrated coherent cross section (see Eqs. (1) and (5)) for the neutrino reactions (10) are illustrated. Figure 1(a)-(c), shows the form factors for protons (F_Z) and neutrons (F_N) obtained with our BCS calculations (for the three isotopes $^{112,114,116}\text{Cd}$) and Fig. 1(d) shows the momentum dependence of $\mathcal{F}(q^2)$ that enters Eqs. (1) and (5).

It should be noted that, the corrections due to the nucleon finite size ($e^{-(qb_N)^2/6}$) and the nuclear center-of-mass motion ($e^{(qb)^2/4A}$), which enter as an overall q -dependent factor in the $F_{N,Z}(q)$, for the medium heavy Cd-isotopes are negligible and have been ignored. The correction due to the nucleon finite size (the larger of the two) is very well known, but not essential. For small q the influence is close to zero while at the maximum momentum q it is about 5% [53].

As can be concluded from Fig. 1, the above ground state properties of the three Cd isotopes studied are to a large extent similar which means that their nuclear structures are not significantly different (all of them have ground state spin $J^\pi = 0^+$). The differences, are mostly due to the small ratio ($\Delta N_i/N \approx 3\% - 6\%$) in their neutron number.

Figure 2 illustrates the total integrated coherent cross sections of ν - $^{112,114,116}\text{Cd}$ scattering as a function of (i) the momentum transfer q , Fig. 2(a), and (ii) the incoming neutrino energy ε_ν , Fig. 2(b). As mentioned before, these original cross sections will be used below for evaluations of flux averaged folded cross sections for various neutrino spectra.

Before closing this section, it is worth mentioning that, in calculating the nuclear form factors $\mathcal{F}(q^2)$, see Fig. 1, in the context of the QRPA method, the estimated er-

Isotope	Z, N	Abundance (%)	b (fm)	g_{pair}^n	g_{pair}^p	Δ_p^{exp}	Δ_p^{th}	Δ_n^{exp}	Δ_n^{th}
^{112}Cd	48, 64	24.13	2.208	1.001	1.064	1.516	1.512	1.320	1.322
^{114}Cd	48, 66	28.73	2.214	0.956	0.975	1.441	1.441	1.351	1.351
^{116}Cd	48, 68	7.50	2.219	1.069	1.043	1.432	1.432	1.371	1.372

TABLE I: Pairing parameters g_{pair}^p (for protons), and g_{pair}^n (for neutrons) determining the monopole pairing interactions for each of the studied isotopes. The obtained theoretical values of the energy gaps (in units of MeV), Δ_p^{th} (for protons) and Δ_n^{th} (for neutrons), are also shown for comparison with the empirical ones. As can be seen, the corresponding empirical energy gaps, $\Delta_{p,n}^{exp}$ are well reproduced. Values of the harmonic oscillator size parameter, b , for each of the isotopes $^{112,114,116}\text{Cd}$ are also given in this Table.

ror at low momentum transfer is very small, while in the momentum range of our interest $0 \leq q \leq 2fm^{-1}$, it is at maximum 10-15%. On the other hand, the experimental accuracy, for the proton form factors entering Eq. (2), usually they come from electron scattering measurements, is of the order of 1% [50]. For neutron form factors, however, the available experimental data are limited and, in general, authors discuss about differences between corresponding proton and neutron nuclear form factors (in medium heavy isotopes like $^{112,114,115}\text{Cd}$) of the order of 4 to 8% [52, 54].

In the next section, we summarize the main features of the ν -energy distributions employed in this work for obtaining folded neutrino-nucleus cross sections for each ν -source.

IV. ENERGY-SPECTRA OF LOW-ENERGY AND INTERMEDIATE ν -SOURCES

In this section, we focus on the basic characteristics of the currently interesting astrophysical (solar-, supernova-, geo-neutrino) and laboratory (reactor neutrino and pion/muon decay at rest neutrino) sources, their energy spectra of which will be used in the convolution procedure (see next section) to obtain convoluted cross sections based on our original cross sections.

In general, the ν -beams of the above mentioned neutrino sources have broad energy distributions (sometimes they consist of a mixture of neutrinos and anti-neutrinos) characteristic of the considered source. Some well known mono-energetic (monochromatic) fluxes are e.g. the one coming out of the charged-pion decay at rest (corresponding to the energy $\varepsilon_{\nu\mu} = 29.65$ MeV, see Fig. 3(d panel). For the non-mono-energetic neutrino fluxes we define the energy distributions $\eta(\varepsilon_\nu)$ as

$$\frac{dN_\nu(\varepsilon_\nu)}{d\varepsilon_\nu} \equiv \eta(\varepsilon_\nu) \quad (12)$$

(N_ν represents the number of neutrinos of the beam).

We note that, via these energy spectra $\eta(\varepsilon_\nu)$ of the specific neutrino sources, the original ν -nucleus cross sections (of neutral-current reactions) computed with

the QRPA method, can be connected with physical observables and signals recorded at the nuclear detectors through the use of the folding (convolution) method described below. The obtained this way folded (convoluted) cross sections represent the simulated nuclear detector response of the $^{112,114,116}\text{Cd}$ isotopes, in the energy range of ν -energy distribution of the studied neutrino source.

The main properties of the aforementioned astrophysical and laboratory neutrinos are summarised in the next subsections.

A. Geoneutrinos

As it is well known, the decay of some radioactive isotopes (mainly U , Th , K) in the interior of our planet, makes the Earth a powerful source of low-energy neutrinos in the range $\varepsilon_\nu \lesssim 10$ MeV [40–43]. Accurate measurements of the flux of these neutrinos [15, 18] are utilized to determine the amount of heat-producing elements in the Earth's mantle. This amount may be compared to that estimated through indirect methods, an information which is important to understand the heat transfer within the Earth. The latter is responsible for earthquakes and volcanoes. The most recent measurements from KamLAND and Borexino [14, 16, 17] are useful to put limits on the parameters of various models describing the structure and evolution of our planet.

The Earth neutrinos (mainly electron anti-neutrinos $\tilde{\nu}_e$), are generated through β -decay processes of neutron-rich nuclei like U , Th and others. These thermonuclear reactions are accompanied by the emission of electrons (e^-) and release of energy Q_β as [40]

$$(A, Z) \rightarrow (A, Z + 1) + e^- + \tilde{\nu}_e + Q_\beta. \quad (13)$$

A and Z denote the mass and atomic (proton) number, respectively, of the initial (parent) nucleus. Part of the decay energy Q_β is carried away by anti-neutrinos (Q_ν) while the remainder is available for heating (Q_h). Thus, $Q_\beta = Q_\nu + Q_h$.

In general, the radioactive isotopes of the Earth are classified into three groups: (i) isotopes in the ^{238}U decay series, (ii) isotopes in ^{232}Th decay series, and (iii)

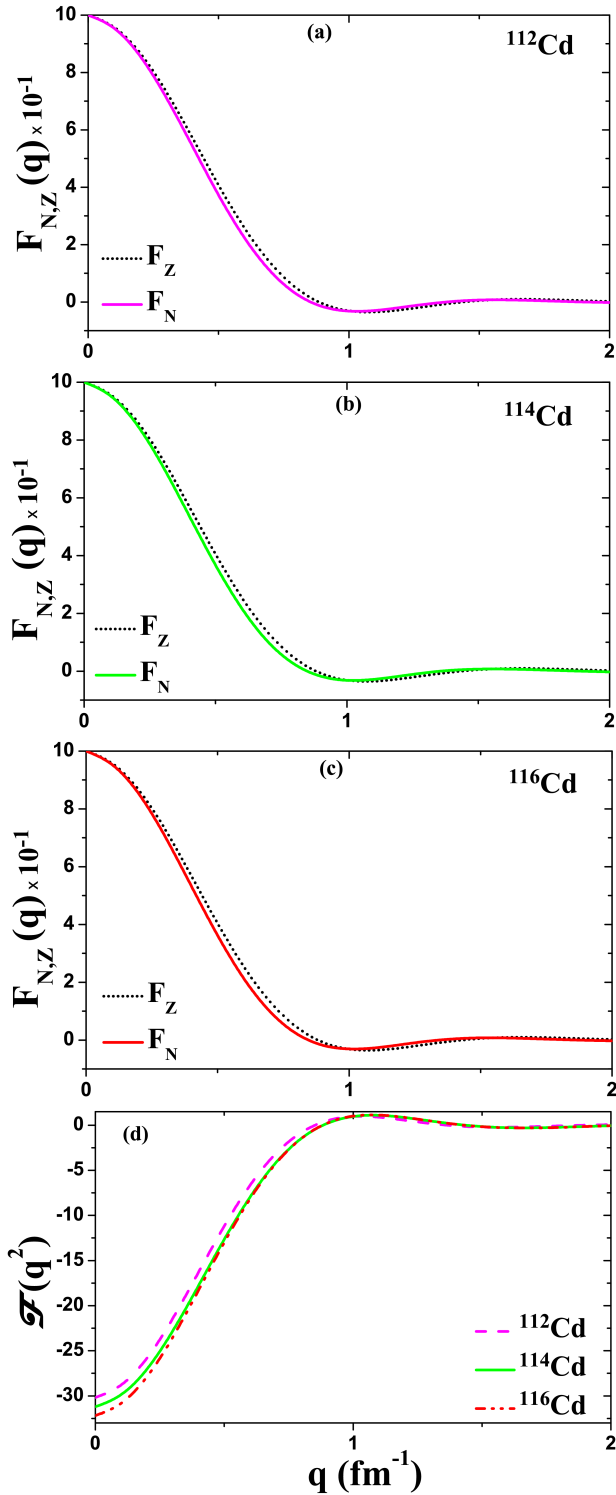


FIG. 1: Neutron and proton nuclear form factors $F_{N,Z}(q^2)$ (a) for ^{114}Cd , (b) for ^{112}Cd , and (c) for ^{116}Cd isotopes. (d) The ground-state elastic nuclear form factor $\mathcal{F}(q^2)$ for $^{112,114,116}\text{Cd}$ isotopes.

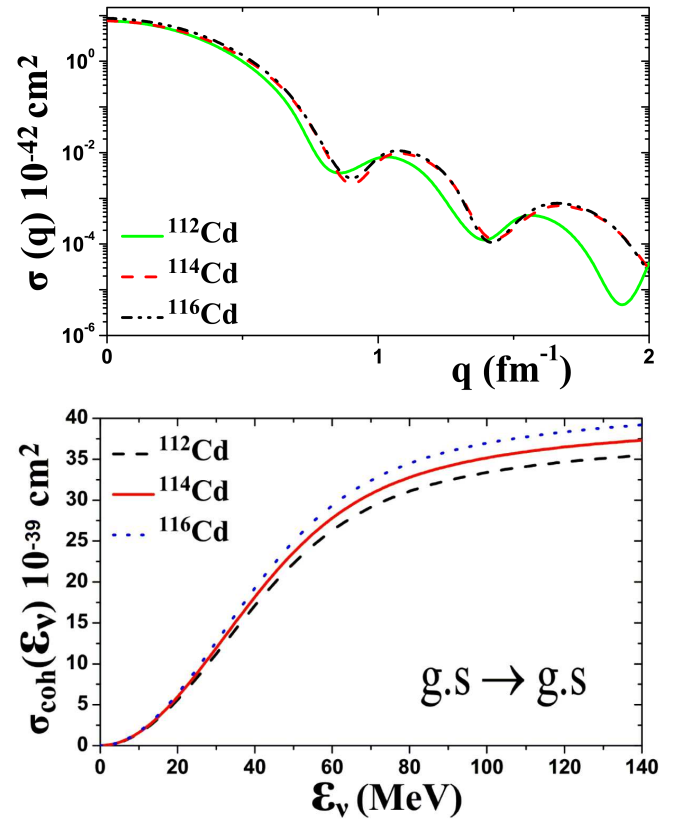


FIG. 2: Total cross sections of coherent (ground state to ground state $g.s. \rightarrow g.s.$) transitions for the neutral current reactions $^{112,114,116}\text{Cd}(\nu_l, \nu_l')^{112,114,116}\text{Cd}^*$, $l = e, \mu, \tau$.

^{40}K isotope [40, 41]. Thus, these isotopes are geologically important because they heat (radiogenic heat) the Earth's interior (finally each of them reaches a stable nuclear isotope) via β -decays of all intermediate radioactive isotopes.

Figure 3(a panel), shows the individual anti-neutrino spectra from ^{40}K , ^{238}U series and ^{232}Th series ($\tau_{1/2} = 4.47 \times 10^9$ y, $\tau_{1/2} = 14.0 \times 10^9$ y and $\tau_{1/2} = 1.28 \times 10^9$ y, respectively). Essentially, these anti-neutrino ($\bar{\nu}_e$) energy spectra come from 82 beta decays in the U series and 70 beta decays in the Th series [40–43, 71, 72].

B. Solar neutrinos

The solar neutrino spectra (mainly ν_e neutrinos) are produced through thermonuclear reactions taking place in the interior of the Sun [73–75]. The shape of the energy distribution ($0.1 \text{ MeV} \leq \mathcal{E}_\nu \leq 18 \text{ MeV}$) depends on the densities and temperatures in the Sun's environment [74] and the individual process of the reaction chain (p-p neutrinos, ^7Be neutrinos, ^8B neutrinos, hep neutrinos, CNO-cycle neutrinos, etc.). In Fig.3(c panel), we show the energy spectra of the important ^8B [73] and hep [55, 74] neutrino sources predicted by the standard so-

lar model [55]. The 8B ν -spectrum, is nearly symmetric, with a peak at 6.4 MeV while the *hep* spectrum is peaked at 9.6 MeV [55].

The detection of the solar neutrinos (produced either via the pp-chain reactions or via the CNO-cycle processes) by terrestrial experiments (SNO+ [17, 19]), constitutes excellent probes for astrophysics, nuclear physics, and particle physics searches [74, 75]. Besides the huge success of the solar-neutrino experiments the last decades, there are still many unsolved questions related to the metallicity of the Sun's core, the total luminosity in neutrinos, the neutrino oscillations, etc. [14, 16, 17, 19, 20].

C. Pion-muon decay at rest neutrino energy distributions

In muon factories (at J-Park, Fermilab, PSI, etc.), from pion and muon decay at rest (DAR), in addition to the monochromatic ν -beam peaked at $\varepsilon_{\nu\mu} = 29.65$ MeV), $\tilde{\nu}_\mu$ and ν_e beams (with energy of a few tens of MeV) are created. Such intermediate energy neutrino sources, are also the currently available at high-intensity proton sources, like the SNS at Oak Ridge, the neutrino beam-line produced at Fermilab Booster, the future Project-X facilities at Fermilab, etc. [14, 16, 17, 19, 20].

In the farther future, such high-intensity muon beams would offer a possible site for neutrino experiments related to supernova neutrinos and for neutrino-nucleus cross section measurements in a great number of nuclei [25, 44–46]. In the operating pion-muon decay at rest neutrino sources (in Fermilab, at USA, J-PARC, at Japan, PSI in Switzerland, etc.) and in the neutrino facilities at the Neutron Spallation Source (Oak Ridge, USA), ν_e neutrinos, and $\tilde{\nu}_\mu$ anti-neutrinos are produced from the decay of muons according to the reaction

$$\mu^+ \rightarrow e^+ + \nu_e + \tilde{\nu}_\mu. \quad (14)$$

The decaying muons result from the decay of pions at rest ($\pi^+ \rightarrow \mu^+ + \nu_\mu$). Thus, these neutrino beams are not completely pure as, for example, the β -beam neutrinos [23, 25]. The energy-spectra of ν_e and $\tilde{\nu}_\mu$ neutrinos are fitted with the normalized distributions [71, 76]

$$\eta_{\nu_e}(\varepsilon_\nu) = 96\varepsilon_\nu^2 M_\mu^{-4} (M_\mu - 2\varepsilon_\nu), \quad (15)$$

$$\eta_{\tilde{\nu}_\mu}(\varepsilon_\nu) = 16\varepsilon_\nu^2 M_\mu^{-4} (3M_\mu - 4\varepsilon_\nu), \quad (16)$$

see Fig. 3(d panel), where $M_\mu = 105.6$ MeV, is the muon rest mass. The $\tilde{\nu}_\mu$ spectrum is peaked at $\varepsilon_{\tilde{\nu}_\mu}^{max} = 52.8$ MeV = $M_\mu/2$ while that of ν_e is peaked at $\varepsilon_{\nu_e}^{max} = 35.2$ MeV = $M_\mu/3$ [7, 76].

Obviously, the analytic expressions of Eqs. (15) and (16), are convenient for the required integrations in the folding procedure, see below [11, 13, 32, 69]. On the other hand, their energy range and shape roughly resembles that of SN neutrinos.

D. Reactor Neutrino spectra

The fission of very heavy nuclear isotopes ${}^{235}U$, ${}^{239}Pu$, and ${}^{238}U$ in the nuclear reactors produces a great number of neutron rich nuclear isotopes. Because these products are unstable, they decay via β -decay emitting anti-neutrinos ($\tilde{\nu}_e$) [77, 78]. Hence, nuclear reactors, operate as intense $\tilde{\nu}_e$ sources for many experiments, giving fluxes of the order of $\sim 10^{13} \tilde{\nu}/\text{cm}^2 \text{ s}$, at distances ~ 10 m from the reactor core.

The energy spectrum of these anti-neutrinos, characteristic of the β^- decay spectrum, is peaked at very low energies ~ 0.3 MeV and covers the energy region below ~ 10 MeV. Figure 3(b panel) illustrates the reactor neutrino spectra normalized so as the sum over all data-points to be equal to unity. The adopted fuel composition is 62% ${}^{235}U$, 30% ${}^{239}Pu$ and 8% ${}^{238}U$ [77, 79].

Currently operating reactor neutrino experiments, like the TEXONO experiment in Taiwan [80, 81], the MINER experiment at the Nuclear Science Center, Texas A&M University (using neutrinos from the TRIGA reactor) [82], are excellent probes of beyond the standard model neutrino physics searches (electromagnetic ν -properties) and coherent ν -nucleus scattering studies.

E. Supernova neutrino spectra

Supernovae (SN) play key role in the development of our Universe, indicated e.g from the fact that modern simulations of galaxies formation cannot reproduce the structure of the galactic disk without considering supernova data. Today, though the physics of core-collapse supernovae is not yet well-understood, investigations of SN neutrinos supply rich information for understanding their dynamics, the mechanism of SN-neutrino emission, etc., and for interpreting the supernova neutrino burst measurements [1, 5, 6]. Multiple physics signatures are expected from a core-collapse explosion in the next supernova observation [21, 42, 43, 46]. The detection of a future galactic supernova will provide invaluable information on the astrophysics of core-collapse explosion while the high statistics of a galactic SN neutrino signal may allow us to unravel the relevant scenarios.

In general, the shape of SN-neutrino energy-distributions is determined by the conditions pertaining during their emission from the collapsing star causing the cooling of the proto-neutron star formed in its center [63, 83–86]. For the energy distribution of SN neutrinos, some authors used available terrestrial neutrino sources with similar energy spectra, like the Neutron Spallation Source neutrinos and the boosted radioactive neutrino beams (beta beam neutrinos), in order to test the response of some ν -detectors to SN neutrinos [44–46]. Recent stellar modelling use analytic expressions that include various effects through a chemical potential parameter in the well-known two-parameter Fermi-Dirac (FD) distribution [87] or through the average ν -energy in the

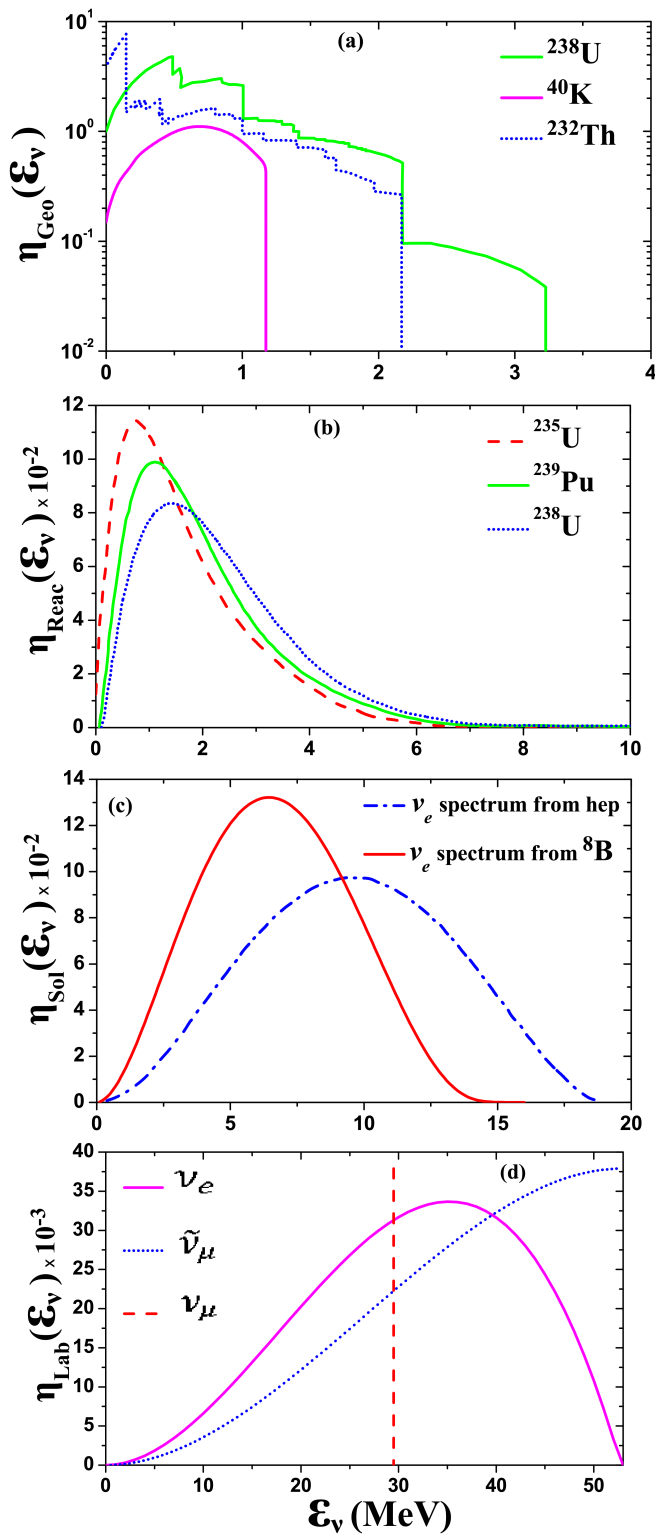


FIG. 3: (a) Spectra of the U-Series, Th-Series and ^{40}K Geo-Neutrinos. Neutrinos from ^{40}K electron capture are also shown in this figure. (b) Normalized reactor neutrino spectra. (c) Normalized energy spectrum of ^8B and hep ν_e solar neutrinos. (d) Energy-spectra of ν_e and $\tilde{\nu}_\mu$ neutrino beams, generated from the muon-decay at rest (see e.g. Refs. [71, 76]).

analytically simpler two parameter Power-Law (PL) distribution (see Appendix) [87–89].

Both parametrizations, FD and PL, yield similar distributions characterized by the temperature T or the average ν -energy $\langle \varepsilon_\nu \rangle$ [13, 69, 90–93]. These analytic normalised expressions contain two parameters to include modulation effects due to various corrections required to modify the purely thermal shape initially employed [87, 88, 91]. The two parameter FD distribution includes the known pinching effect through the degeneracy parameter (the chemical potential divided by the neutrino temperature T), $n_{dg} = \mu/T$ which makes the spectrum more narrow compared to the purely thermal shape of temperature T (in MeV) [13]. The two parameter PL distribution of SN- ν energy spectrum [88, 89], contains as parameters the mean neutrino energy $\langle \varepsilon_\nu \rangle$ and the parameter α which adjusts the width w of the distribution [13, 87, 88, 91] (see Appendix).

In Fig. 4, some flavour dependent ν -energy spectra (η_{SN}) emitted by a core-collapse Supernova, needed for our present work, are illustrated. Both FD and PL energy distributions (labelled η_{FD} and η_{PL} , respectively) are shown for three different values of the width parameter $w = 0.7$, $w = 0.8$ and $w = 0.9$ (see Appendix) and for five equivalent parametrizations. From the FD distributions (with parameters the temperature T and the width parameter w), we see that, as the temperature grows the maximum of the distribution shifts to larger ν -energy (at the same time the corresponding peak becomes smaller). Also, as the width parameter w grows (keeping the same temperature), both the maximum of the distribution shifts to smaller ε_ν and its peak becomes smaller. Furthermore, the degeneracy parameter shifts the spectrum to higher energies [13, 91]. In this figure, the PL energy distributions for the corresponding values of mean neutrino energy $\langle \varepsilon_\nu \rangle$, are also illustrated ($\langle \varepsilon_\nu \rangle$ reflects the depth of the stars from which the neutrinos are escaping. We see that, as the $\langle \varepsilon_\nu \rangle$ grows, the maximum of the distribution shifts to higher ν -energy ε_ν [88, 91].

In Table II, the corresponding values of parameters for the equivalent FD and PL ν -energy spectra of Fig. 4, that have been employed in various SN scenarios are shown (for more details see the Appendix and Ref. [13]). It is worth mentioning that, due to neutrino oscillations and other phenomena, at any distance from the source the SN- ν spectra can be different compared to those originally produced at the core of the collapsing star. It is, however, expected that ν -signals with much higher statistics from future galactic SN, may allow us to assess the great number of neutrino mixing scenarios.

It is worth mentioning that, the statistics for the SN 1987A were rather poor, just a few dozen $\tilde{\nu}_e$ events were received within about ten seconds. For the observation of the next core-collapse SN-neutrino burst, however, detectors with huge statistics and remarkably greater flavour sensitivity are in operation or have been planned to operate in the near future [94]. Among those, are the next generation detectors HyperKamiokande, Juno,

Equivalent Fermi-Dirac and Power-Law Supernova Neutrino Spectra							
Parameter			Temperature (in MeV)				
Width (w)	Pinching (α)	Degeneracy (n_{dg})	$\langle \varepsilon_\nu \rangle = 10$	$\langle \varepsilon_\nu \rangle = 12$	$\langle \varepsilon_\nu \rangle = 16$	$\langle \varepsilon_\nu \rangle = 20$	$\langle \varepsilon_\nu \rangle = 24$ (MeV)
0.7	5.1	4.4	2.14	2.57	3.42	4.28	5.13
0.8	3.7	2.7	2.58	3.10	4.14	5.17	6.20
0.9	2.7	1.1	2.98	3.57	4.77	5.96	7.15

TABLE II: Corresponding values of parameters for equivalent Fermi-Dirac (FD) and Power-Law (PL) distributions (SN neutrino energy spectra) of Fig. 4. The selected flavour dependent mean ν -energy values (describing the PL distribution), $\langle \varepsilon_\nu \rangle$ in MeV, have been chosen as model values for ν_e (10-12) MeV, $\bar{\nu}_e$ (15-18) MeV and ν_x , where $x = \nu_\mu, \nu_\tau, \bar{\nu}_\mu, \bar{\nu}_\tau$ (22-26) MeV.

Dune, etc., which aim at measuring, among others, the diffuse SN neutrino background [95, 96].

V. SIMULATED NEUTRINO SIGNALS ON NUCLEAR DETECTORS

The features of a neutrino-flux that arrives at a neutrino detector are concealed in the nuclear response of the detector-material. In the case of the COBRA detector, the semi-conductor materials CdTe or CdZnTe contain large portion of Cd isotopes [3, 4, 26]. Our aim in this section is to simulate some of these features by calculating convoluted cross sections as discussed in Refs. [13, 32].

The convolution (folding) is carried out with (i) the original cross sections obtained in Sect. III, and (ii) the low and intermediate energy neutrino spectra of Section IV in order to compute, first, flux averaged total cross sections, $\langle \sigma_{tot} \rangle$ and, then, corresponding supernova neutrino event rates and fluxes.

A. Flux averaged cross sections for Cd detector materials

For the coherent channel, which is possible only in neutral current neutrino-nucleus reactions studied in this work, the flux averaged cross section $\langle \sigma_{coh} \rangle$ is obtained through the folding [6, 11, 13]

$$\langle \sigma_{coh} \rangle = \int_0^\infty \sigma_{coh}(\varepsilon_\nu) \eta(\varepsilon_\nu) d\varepsilon_\nu. \quad (17)$$

For a CdTe or CdZnTe detector material, the flux averaged cross sections, computed by inserting in Eq. (17) the $\sigma_{coh}(\varepsilon_\nu)$ from Fig. 2(b) and the $\eta(\varepsilon_\nu)$ from Figs. 3 and 4, for the isotopes $^{112,114,116}\text{Cd}$, are listed in Tables III and IV as described below.

In Table III we list the flux averaged cross sections evaluated by adopting the neutrino distributions of the geo-neutrinos (see Fig. 3(a)), the reactor neutrinos (see

Fig. 3(b)) and the solar neutrinos (see Fig. 3(c) for the ^8B and the *hep* solar neutrinos).

In the last two columns of Table IV we tabulate the $\langle \sigma_{coh} \rangle$ calculated for the distributions of Eqs. (15) and (16), i.e. the ν -spectra produced by pion/muon decay at rest (DAR). In the first three columns of this Table, the flux averaged cross sections refer to various supernova neutrino scenarios described by the equivalent FD and PL distributions of Fig. 4. The corresponding parameters are listed in Table II.

In supernova neutrino scenarios, usually average ν -energies between $10 \leq \langle \varepsilon_\nu \rangle \leq 12$ MeV are employed for the description of ν_e neutrinos, average energies between $15 \leq \langle \varepsilon_\nu \rangle \leq 18$ MeV for $\bar{\nu}_e$ anti-neutrinos, and average energies between $22 \leq \langle \varepsilon_\nu \rangle \leq 26$ MeV for ν_x and $\bar{\nu}_x$, with $x = \mu, \tau$ [87–89, 91].

Due to the dominance of the coherent channel throughout the region of the incoming neutrino energy ε_ν of our present calculations, the flux averaged coherent cross section $\langle \sigma_{coh} \rangle$ may be even two or three orders of magnitude larger than the total incoherent cross section $\langle \sigma_{tot}^{incoh} \rangle$ [11, 13, 69].

B. Number of events in ν -detectors

The present theoretical results may be connected with current neutrino experiments relying on Cd isotopes as detection materials, and specifically the COBRA experiment at Gran Sasso [3, 4, 26], as follows. By using the flux averaged cross sections $\langle \sigma(\varepsilon_\nu) \rangle$ of Table IV, for instance those referred to the SN neutrinos of the $^{112,114,116}\text{Cd}$ isotopes, we estimate (potentially detectable) neutrino fluxes Φ_ν that should arrive at each detector to create some typical scattering event rates N_{ev} in the COBRA detector.

In general, the event rate N_{ev} is related to the flux Φ_ν reaching the nuclear detector with the expression [11, 32, 70]

$$\frac{dN_\nu}{dt} \equiv N_{ev} = N_{Cd} \sigma_{tot}(\varepsilon_\nu) \Phi_\nu(\varepsilon_\nu). \quad (18)$$

Flux Averaged Cross Sections $\langle\sigma_{coh}\rangle$ (10^{-39} cm^2)								
	Geo-Neutrinos			Reactor Neutrinos			Solar Neutrinos	
Isotope	^{40}K	^{238}U	^{232}Th	^{235}U	^{238}U	^{239}Pu	^8B	hep
^{112}Cd	0.142	1.410	0.911	0.180	0.477	9.001	7.970	9.333
^{114}Cd	0.151	1.504	0.973	0.192	0.509	9.604	8.504	9.957
^{116}Cd	0.161	1.602	1.036	0.205	0.542	1.023	9.055	10.598

TABLE III: Calculated values for the flux averaged coherent cross sections $\langle\sigma_{coh}\rangle$ (in units 10^{-39} cm^2) for ^{112}Cd , ^{114}Cd and ^{116}Cd isotopes. The neutrino sources distributions of neutrino beams coming from: (i) Geo-neutrinos, (ii) Reactor neutrinos and (iii) Solar neutrinos have been used in the folding procedure.

Flux Averaged Cross Sections $\langle\sigma_{coh}\rangle$ (10^{-39} cm^2)										
Isotope	Supernova Neutrinos						Pion-muon DAR Neutrinos			
	Fermi-Dirac (FD)			Power Law (PL)			ν_e Spect.	$\tilde{\nu}_\mu$ Spect.		
	$T =$	3.10	4.14	6.20	$\langle\varepsilon_\nu\rangle =$	12	16	24		
^{112}Cd		2.484	4.184	8.132		2.489	4.180	8.142	12.338	14.960
^{114}Cd		2.648	4.458	8.648		2.653	4.453	8.658	13.110	15.881
^{116}Cd		2.817	4.739	9.178		2.823	4.734	9.189	13.801	16.824

TABLE IV: Flux averaged coherent cross sections $\langle\sigma_{coh}\rangle$, as in Table III but now referred to: (i) three different Supernova neutrino spectra determined from the parameters of: (a) Fermi Dirac parametrizations and (b) Power-Law parametrizations, and (ii) the energy spectra of Pion/muon decay at rest (DAR) neutrinos.

We note that, experimentalists use the definition

$$N_{ev} = \epsilon N_{Cd} \sigma_{tot}(\varepsilon_\nu) \Phi_\nu(\varepsilon_\nu),$$

which takes into account the detection efficiency ϵ (usually equal to $\epsilon \approx 80 - 90\%$) of the specific detector. Here, we assume a COBRA detector of mass $m_{det}=100$ kg and two cases of detector materials, i.e the semiconductors (a) CdZnTe and (b) CdTe [3, 4, 26].

In the first step, we choose three SN neutrino scenarios in which the mean energies are: (i) $\langle\varepsilon_\nu\rangle = 12$ MeV (corresponding to SN electron neutrinos ν_e), (ii) $\langle\varepsilon_\nu\rangle = 16$ MeV (corresponding to SN electron anti-neutrinos $\tilde{\nu}_e$), and (iii) $\langle\varepsilon_\nu\rangle = 24$ MeV (corresponding to SN ν_x , $\tilde{\nu}_x$, with $x = \mu, \tau$ (anti)neutrinos of heavy leptons).

Then, based on Eq. (18), we perform calculations assuming a total mass 100 kg of CdZnTe as COBRA detector which translates, for example, to approximately $m_{Cd} = 10.6$ kg mass of ^{114}Cd isotope or equivalently a number of ^{114}Cd atoms (nuclei) equal to $N_{Cd} \equiv N_{114Cd} = 94.17 N_{Avog}$.

In Eq. (18), as total neutrino scattering cross sections, $\sigma_{tot}(\varepsilon_\nu)$ we employ the values of flux averaged cross sections $\langle\sigma_{coh}\rangle$ of Table IV obtained through PL distribution for SN neutrino spectra (they refer to the three mean energies chosen above).

Finally, we choose four typical detection rates N_{ev} as: (a) $N_{ev}=1$ event $\text{s}^{-1}=3.15\times 10^7$ events y^{-1} , (b) $N_{ev}=1$ event $\text{hr}^{-1}=8.76\times 10^3$ events y^{-1} , (c) $N_{ev}=1$ event $\text{d}^{-1}=3.65\times 10^2$ events y^{-1} , and (d) $N_{ev}=12$ events y^{-1} and (from Eq. (18) we compute the corresponding SN ν fluxes Φ_ν .

In a similar way, assuming that the COBRA detector contains 100 kg of the material CdTe, we find 13.5 kg ^{114}Cd or about $N_{Cd} \equiv N_{114Cd} = 120.11 N_{Avog}$ atoms (nuclei) are contained in the second semiconductor material of COBRA detector. By performing similar calculations for the same SN scenarios and the same, as before, set of detection rates N_{ev} , we find the corresponding fluxes Φ_ν reaching the COBRA CdTe detector.

By performing the steps we followed for ^{114}Cd , for the

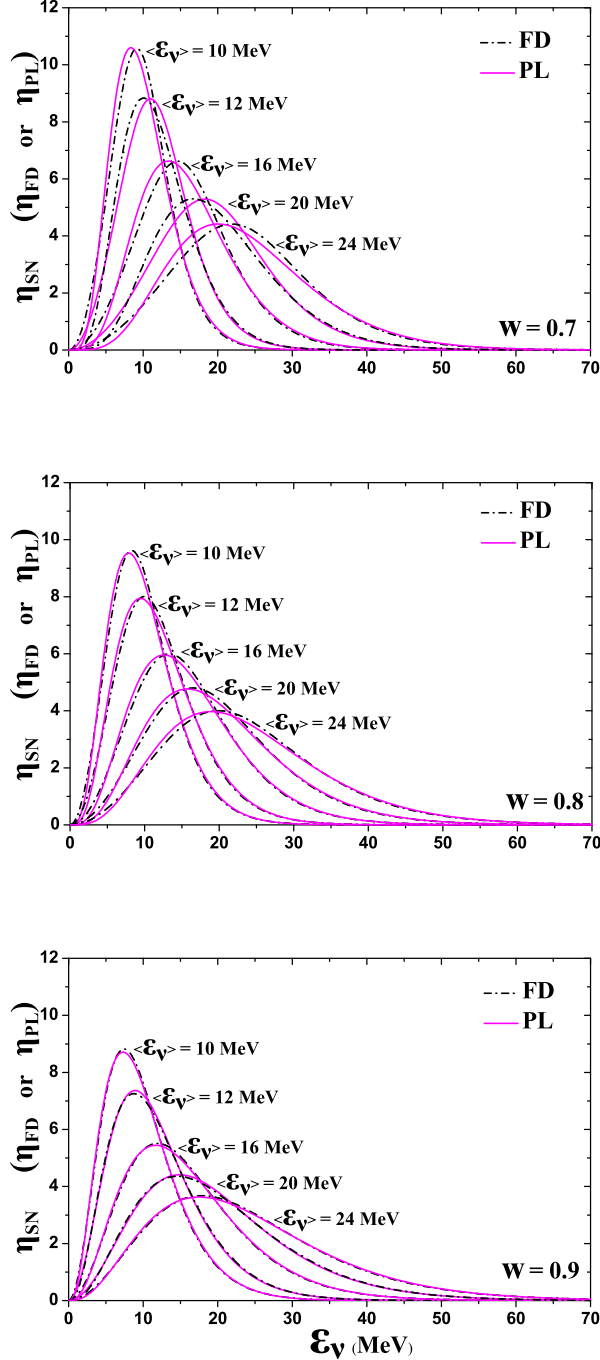


FIG. 4: Supernova neutrino energy spectra (η_{SN}) coming out of the analytic expressions of: (i) the two-parameter Fermi-Dirac distribution (FD) and (ii) the two-parameter Power-law (PL) distribution (see Appendix). The five sets of values of their parameters refer to equivalent distributions (for details see the text).

other two Cd-isotopes, ^{112}Cd and ^{116}Cd , the resulting neutrino fluxes, for the chosen SN neutrino scenarios are listed in Table V (last four columns). Such results are useful for future use of the Cd materials in astrophysical neutrino detection. It should be stressed that, next generation experiments may be effective in the detection of much weaker signals (higher sensitivity, larger detector mass, etc.).

The above neutrino fluxes are of the same order with those of the Spallation Neutron Source (SNS) at ORNL, Oak Ridge [44–46]. We mention that the COHERENT experiment at Oak Ridge, with a 14.57 kg of CsI scintillator detector, by using an SNS ν_μ neutrino flux (coming from π -decay at rest) as high as $\Phi_\nu^{COH} = 1.7 \times 10^{11} \nu_\mu/cm^2 s$, has measured 142 CEvNS events within a period of 308.1 live days (at a distance of $L = 19.3$ m from the source) [8]. These results translate to event rate $N_{ev}^{COH} = 168/y \nu_\mu$ neutrinos.

From the results of Table V, we may define the ratio N_{ev}/Φ_ν for the COHERENT experiment (R^{COH}) and for a special ν_μ neutrino case of the COBRA experiment (R^{COB}). For a comparison of these two experiments, we choose, for example, the results referred to the ^{112}Cd isotope of CdTe material of the COBRA detector (sixth line from the beginning of Table V refers to ν_μ neutrinos). From these two ratios we find that $R = R^{COH}/R^{COB} = 98.95/2.94 \approx 34$, which means that, for the chosen SN neutrino scenario, the COBRA detector may observe 12 ν_μ/y only if its mass is equal to $m \sim 34$ times larger than the assumed above 100 kg, i.e. only if the COBRA detector has a huge total mass $m_{det} = 3.4$ t CdTe material (we mention that, in the assumed scenario, the SN ν_μ neutrinos correspond a Temperature $T=24$ MeV, see one before last column of Table V). This example indicates also the corresponding cost for detector improvement so as to be able to record neutrino signals coming from interesting astrophysical sources.

We should finally note that, in this work the detection efficiency ϵ has not been considered (equivalently we assumed $\epsilon = 1$). Also, the neutrino mixing has not been accounted for which means that we assumed the neutrino spectra arrived at the nuclear detector are described by PL distributions (as in stars interior) of the same values of the parameters.

VI. SUMMARY AND CONCLUSIONS

In this work, we present original neutrino-nucleus cross sections obtained with realistic nuclear structure calculations (use of the QRPA method) for scattering of low and intermediate energy neutrinos off the $^{112,114,116}\text{Cd}$ isotopes. These Cd-isotopes are contents (with large abundance) of the detector materials of the COBRA detector at Gran Sasso. The neutrino energy assumed covers currently interesting laboratory (reactor, pion/muon decay at rest neutrinos) and Astrophysical (solar, super-

Supernova neutrino coherent fluxes Φ_ν ($s^{-1} cm^{-2}$) and event rates N_{ev}									
					$N_{ev} = 1/s$	$N_{ev} = 1/hr$	$N_{ev} = 1/d$	$N_{ev} = 12/y$	$N_{ev}^{COH} = 168/y$
Isotope	Detector	Atoms (N_{Avog})	m (kg)	$\langle\varepsilon_\nu\rangle$ (MeV)	$\Phi_\nu(\times 10^5)$	$\Phi_\nu(\times 10^9)$	$\Phi_\nu(\times 10^{10})$	$\Phi_\nu(\times 10^{11})$	$\Phi_\nu^{COH}(\times 10^{11})$
^{112}Cd	CdTe	100.08	11.25	12	5.14	1.85	4.44	13.33	1.70
				16	3.06	1.10	2.65	7.94	
				24	1.57	0.57	1.36	4.08	
^{112}Cd	CdZnTe	100.05	11.25	12	5.15	1.85	4.45	13.34	1.70
				16	3.06	1.10	2.64	7.94	
				24	1.57	0.57	1.36	4.08	
^{114}Cd	CdTe	121.29	13.50	12	3.98	1.45	3.44	10.32	1.70
				16	2.37	0.86	2.05	6.15	
				24	1.22	0.45	1.05	3.16	
^{114}Cd	CdZnTe	121.26	10.60	12	4.26	1.85	3.67	11.00	1.70
				16	2.53	1.10	2.18	6.55	
				24	12.98	0.57	1.12	3.36	
^{116}Cd	CdTe	32.18	3.62	12	14.10	5.08	12.19	36.56	1.70
				16	8.41	3.03	7.27	21.80	
				24	4.33	1.56	3.74	11.23	
^{116}Cd	CdZnTe	32.18	3.62	12	16.00	5.76	13.83	41.48	1.70
				16	9.53	3.43	8.23	24.70	
				24	4.89	1.76	4.23	12.66	

TABLE V: Neutrino fluxes $\Phi_\nu(\varepsilon_\nu)$ and corresponding event rates N_{ev} estimated to be recorded on $^{112,114,116}\text{Cd}$ isotopes of two detector materials (CdTe and CdZnTe) of the COBRA experiment [3, 4, 26]. They refer to the case of supernova neutrinos with mean energies $\langle\varepsilon_\nu\rangle = 12, 16$ and 24 MeV. N_{Avog} is the Avogadro's number. In the last column, N_{ev}^{COH} and Φ_ν^{COH} describe COHERENT experiment values (see the text).

nova and Earth) neutrino sources. Laboratory neutrino beams are important tools for studying standard and non-standard neutrino physics while astrophysical neutrinos are key particles in investigating the structure and evolution of stars as well to deepen our knowledge on the fundamental neutrino-nucleus interactions.

By utilizing the convolution procedure, we calculated flux averaged cross sections and event rates for the above ν -sources based on specific spectral distributions describing supernova neutrino energy spectra, solar neutrinos, geo-neutrinos and laboratory neutrinos as well as reactor neutrinos and pion-muon-stopped neutrinos. The flux-averaged total coherent cross sections, $\langle\sigma_{coh}\rangle$, reflect the mean neutrino signals generated in several terrestrial detectors ($^{112,114,116}\text{Cd}$) from such ν -sources. Important connection of our present results with current experiments may also be achieved through the evaluation of the neutrino scattering event rates on Cd detectors.

The estimated neutrino fluxes and scattering event rates for Cd-isotopes, contents of the CdTe and CdZnTe materials of the COBRA detector at LNGS, may support this experiment to reach its goal in searching for neutrino observation and detection of rare events (double beta decay, etc).

VII. ACKNOWLEDGEMENTS

The present research was financially supported (V. Tsakstara and J. Sinatkas) by the Department of Informatics Engineering of the Technological Institute of Western Macedonia. Also, Dr. Odysseas Kosmas wishes to acknowledge the support of EPSRC via grand EP/N026136/1 "Geometric Mechanics of Solids".

Appendix

A. Three-point formulas for empirical energy gaps $\Delta_{n,p}^{exp}$ of neutrons and protons

The empirical energy gaps for neutrons, Δ_n^{exp} , and protons, Δ_p^{exp} , needed at the BCS level to construct the ground state wave function of the detector nucleus (A, Z), are computed through the respective separation energies for neutrons, S_n or protons, S_p of the isotope (A, Z) and also those of the neighbouring nuclear isotopes with $N \pm 1$ neutrons or $Z \pm 1$ protons, respectively, by employing the expressions

$$\Delta_n^{exp} = -\frac{1}{4}[S_n(N-1, Z) - 2S_n(N, Z) + S_n(N+1, Z)] \quad (19)$$

$$\Delta_p^{exp} = -\frac{1}{4}[S_p(N, Z-1) - 2S_p(N, Z) + S_p(N, Z+1)] \quad (20)$$

The above equations are known as the three-point formulas (see, e.g. Ref. [69, 97]).

B. Normalization of the ν energy distributions $\eta(\varepsilon_\nu)$ adopted in this work

The distributions $\eta(\varepsilon_\nu)$ adopted in the present work (see Sect. IV), are considered to be normalized in such a way that

$$\int_0^\infty \eta(\varepsilon_\nu) d\varepsilon_\nu = 1. \quad (21)$$

For example, in the case of $\eta_{\nu_e}(\varepsilon_\nu)$ of Fig. 3(d), the normalization gives

$$(96/M_\mu^4) \left[M_\mu \int_0^{M_\mu/2} \varepsilon_\nu^2 d\varepsilon_\nu - 2 \int_0^{M_\mu/2} \varepsilon_\nu^3 d\varepsilon_\nu \right] = 1$$

where we have used $\varepsilon_\nu^{min} = 0$ and $\varepsilon_\nu^{max} = M_\mu/2$

C. Parametrization of Supernova neutrino energy spectra

The Fermi-Dirac (FD) and Power-law (PL) energy distribution are commonly used in Supernova neutrino parametrizations. Both the FD and PL yield very similar distributions characterized by the temperature T or the average energy $\langle \varepsilon_\nu \rangle$ and the width w of the spectrum is defined as

$$w = \sqrt{\langle \varepsilon_\nu^2 \rangle - \langle \varepsilon_\nu \rangle^2} / w_0$$

where $w_0 = \varepsilon_\nu / \sqrt{3}$ is the width of the identical FD and PL distributions [13].

1. Fermi-Dirac (FD) energy distribution

By introducing the degeneracy parameter n_{dg} (equal to the ratio of the chemical potential μ divided by the neutrino temperature T , i.e. $n_{dg} = \mu/T$), the Fermi-Dirac energy distribution reads

$$\eta_{FD}[x, T, n_{dg}] = F(n_{dg}) \frac{1}{T} \frac{x^2}{1 + e^{(x-n_{dg})}}, \quad x = \frac{\varepsilon_\nu}{T}. \quad (22)$$

In this case, the width of the spectrum is reduced compared to the corresponding thermal spectrum (pinching effect). The normalization constant $F_2(n_{dg})$ of this distribution depends on the degeneracy parameter n_{dg} and is given by the relation

$$\frac{1}{F(n_{dg})} \equiv \int_0^\infty \frac{x^2}{e^{x-n_{dg}} + 1} dx. \quad (23)$$

Inserting Eq. (23) into Eq. (22), we take

$$\eta_{FD}[\varepsilon_\nu, T, n_{dg}] = \left[\int_0^\infty \frac{x^2}{e^{x-n_{dg}} + 1} dx \right]^{-1} \frac{(\varepsilon_\nu^2/T^3)}{1 + e^{(\varepsilon_\nu/T - n_{dg})}}. \quad (24)$$

2. Power-law energy distribution

The SN-neutrino energy spectra can be fitted by using a Power-Law energy distribution of the form [88]

$$\eta_{PL}[\langle \varepsilon_\nu \rangle, \alpha] = C \left(\frac{\varepsilon_\nu}{\langle \varepsilon_\nu \rangle} \right)^\alpha e^{-(\alpha+1)(\varepsilon_\nu/\langle \varepsilon_\nu \rangle)}, \quad (25)$$

where $\langle \varepsilon_\nu \rangle$ is the neutrino mean energy. The parameter α adjusts the width of the spectrum (see text). The normalization factor C , is calculated from the normalization condition

$$C \int_0^\infty \left(\frac{\varepsilon_\nu}{\langle \varepsilon_\nu \rangle} \right)^\alpha e^{-(\alpha+1)(\varepsilon_\nu/\langle \varepsilon_\nu \rangle)} d\varepsilon_\nu = 1. \quad (26)$$

From the later equation we find

$$C = \frac{(\alpha+1)^{\alpha+1}}{\Gamma(\alpha+1) \langle \varepsilon_\nu \rangle}, \quad (27)$$

therefore, Eq. (25) becomes

$$\eta_{PL}[\langle \varepsilon_\nu \rangle, \alpha] = \frac{(\alpha+1)^{\alpha+1}}{\Gamma(\alpha+1)} \frac{\varepsilon_\nu^\alpha}{\langle \varepsilon_\nu \rangle^{\alpha+1}} e^{-(\alpha+1)(\varepsilon_\nu/\langle \varepsilon_\nu \rangle)}. \quad (28)$$

[1] H. Ejiri, Nuclear spin isospin responses for low-energy neutrinos, Phys. Rep. (2000) **338**:265–351.
 [2] H. Ejiri, J. Engel, N. Kudomi, Supernova-neutrino studies with ^{100}Mo , Phys. Lett. B (2002) **530**:27–32.
 [3] K. Zuber, COBRA-double beta decay searches using CdTe detectors, Phys. Lett. B (2001) **519**:1–7.

[4] K. Zuber, Spectroscopy of low energy solar neutrinos using CdTe detectors, Phys. Lett. B (2003) **571**:148–154.
 [5] T.W. Donnelly and R.D. Peccei, Neutral current effects in nuclei, Phys. Rep. (1979) **50**:185.
 [6] T.S. Kosmas and E. Oset, Charged current neutrino-nucleus reaction cross sections at intermediate energies,

- Phys. Rev. C (1996) **53**:1409–1415.
- [7] E. Kolbe and T.S. Kosmas, Recent highlights on neutrino-nucleus interactions, Springer Trac. Mod. Phys. (2000) **163**:199–225.
- [8] D. Akimov *et al.*, Observation of coherent elastic neutrino-nucleus scattering, Science (2017) **357**:1123–1126.
- [9] K. Scholberg, Prospects for measuring coherent neutrino-nucleus elastic scattering at a stopped-pion neutrino source, Phys. Rev. D (2006) **73**:033005-1–9.
- [10] K. Scholberg, Coherent elastic neutrino-nucleus scattering, J. Phys. Conf. Ser. (2015) **606**:012010-1–10.
- [11] V. Tsakstara and T.S. Kosmas, Low-energy neutral-current neutrino scattering on $^{128,130}\text{Te}$ isotopes, Phys. Rev. C (2011) **83**:054612-1–13.
- [12] V. Tsakstara, T.S. Kosmas, J. Wambach, Studying low-energy astrophysical neutrinos with neutrino nucleus cross-section calculations and beta beam neutrino spectra, Prog. Part. Nucl. Phys. (2011) **66**:424–429.
- [13] V. Tsakstara and T.S. Kosmas, Analyzing astrophysical neutrinos through realistic nuclear structure calculations and the convolution procedure, Phys. Rev. C (2011) **84**:064620-1–14.
- [14] S. Abe *et al.*, Precision Measurement of Neutrino Oscillation Parameters with KamLAND (KamLAND Collaboration), Phys. Rev. Lett. (2008) **100**:221803-1–5.
- [15] A. Gando *et al.*, Partial radiogenic heat model for Earth revealed by geoneutrino measurements (KamLAND Collaboration), Nature Geo. (2011) **4**:647–651.
- [16] G. Bellini *et al.*, Observation of Geo-Neutrinos (Borexino Collaboration), Phys. Lett. B (2010) **687**:299–304.
- [17] G. Bellini *et al.*, Precision Measurement of the ^7Be Solar Neutrino Interaction Rate in Borexino (Borexino Collaboration), Phys. Rev. Lett. (2011) **107**:141302-1–5.
- [18] G. Bellini *et al.*, Measurement of geo-neutrinos from 1353 days of Borexino (Borexino Collaboration), Phys. Lett. B (2013) **722**:295–300.
- [19] K. Zuber, Status of the double beta experiment COBRA, Prog. Part. Nucl. Phys. (2006) **57**:235–240.
- [20] M. Wurm *et al.*, The next-generation liquid-scintillator neutrino observatory LENA, Astropart. Phys. (2012) **35**:685–732.
- [21] E. Kolbe, K. Langanke, G. Martinez-Pinedo, and P. Vogel, Neutrino-nucleus reactions and nuclear structure, J. Phys. G (2003) **29**:2569–2596.
- [22] M.Sajjad Athar and S.K. Singh, $\nu_e(\bar{\nu}_e)-^{40}\text{Ar}$ absorption cross sections for supernova neutrinos, Phys. Lett. B (2004) **591**:69–75.
- [23] P. Zucchelli, A novel concept for a $\bar{\nu}_e/\nu_e$ neutrino factory: the beta-beam, Phys. Lett. B (2002) **532**:166–172.
- [24] C. Volpe, What about a beta beam facility for low-energy neutrinos?, J. Phys. G. (2004) **30**:L1–L6 .
- [25] C. Volpe, Topical Review on Beta-beams, J. Phys. G (2007) **34**:R1–R44.
- [26] K. Zuber, The status of the COBRA double-beta-decay experiment, Prog. Part. Nucl. Phys. (2010) **64**:267–269.
- [27] T. Smponias, O.T. Kosmas, High Energy Neutrino Emission from Astrophysical Jets in the Galaxy, Advances in High Energy Physics (2015) Article ID 921757.
- [28] T. Smponias, O.T. Kosmas, Neutrino Emission from Magnetized Microquasar Jets, Advances in High Energy Physics (2017) Article ID 4962741.
- [29] O.T. Kosmas, T. Smponias, Simulations of Gamma-Ray Emission from Magnetized Microquasar Jets (2018) Article ID 9602960.
- [30] M. G. Aartsen *et al.*, Search for Prompt Neutrino Emission from Gamma-Ray Bursts with IceCube (IceCube Collaboration), Astrophys. J. Lett. (2015) **805**:L5.
- [31] S. Adrian-Martinez *et al.*, Letter of intent for KM3NeT 2.0 (KM3Net Collaboration), J. Phys. G: Nucl. Part. Phys. (2016) **43**:084001-(130pp).
- [32] V. Tsakstara, Convolutd-Signals on ^{114}Cd Isotope from Astrophysical and Laboratory Neutrino Sources, Advances in High Energy Physics (2015) Article ID 632131.
- [33] T.S. Kosmas, J.D. Vergados, O. Civitarese, and Amand Faessler, Study of the muon number violating (μ^- , e^- conversion in a nucleus by using quasi-particle RPA, Nucl. Phys. A (1994) **570**:637–656.
- [34] T.S. Kosmas, Exotic $\mu^- \rightarrow e^-$ conversion in nuclei: energy moments of the transition strength and average energy of the outgoing e^- , Nucl. Phys. A (2001) **683**:443–462.
- [35] I.G. Tsoulos, O.T. Kosmas, and V.N. Stavrou, Dirac-Solver: A tool for solving the Dirac equation, Computer Physics Communications (2019) **236**:237–243.
- [36] O. Kosmas and S. Leyendecker, Analysis of higher order phase fitted variational integrators, Advances in Computational Mathematics (2016) **42**:605–619.
- [37] O. Kosmas and S. Leyendecker, Variational integrators for orbital problems using frequency estimation, Advances in Computational Mathematics (2019) **45**:1–219.
- [38] O. Kosmas and D. Papadopoulos, Multisymplectic structure of numerical methods derived using non standard finite difference schemes, Journal of Physics: Conference Series **490**:012205.
- [39] O.T. Kosmas, Charged Particle in an Electromagnetic Field Using Variational Integrators, AIP Conference Proceedings (2011) **1389**:1927.
- [40] P. Vogel and J.F. Beacom, Angular distribution of neutron inverse beta decay $\bar{\nu}_e + \bar{p}e^+ + n$, Phys. Rev. D (1999) **60**:053003-1–10.
- [41] S. Dye, Geoneutrinos and the radioactive power of the Earth, Rev. Geophys. (2012) **50**:3007.
- [42] G. Fiorentini, E. Mantovani, and B. Ricci, Neutrinos and energetics of the Earth, Phys. Lett. B (2003) **557**:139–146.
- [43] G. Fiorentini *et al.*, Nuclear physics for geo-neutrino studies, Phys. Rev. C (2010) **81**:034602-1–9.
- [44] F.T. Avignone and Y.V. Efremenko, ORLaND - a neutrino facility at the Spallation Neutron Source, Nucl. Phys. B (Proc. Supl.) (2000) **87**:304–308 .
- [45] F.T. Avignone and Y.V. Efremenko, Neutrino-nucleus cross-section measurements at intense, pulsed spallation sources, J. Phys. G (2003) **29**:2615–2628.
- [46] R.L. Burman and W.C. Louis, Neutrino physics at meson factories and spallation neutron sources, J. Phys. G (2003) **29**:2499–2512.
- [47] D.K. Papoulias and T. S. Kosmas, Nuclear aspects of neutral current non-standard ν -nucleus reactions and the role of the exotic $\mu^- \rightarrow e^-$ transitions experimental limits, Phys. Lett. B (2014) **728**:482–488.
- [48] D.K. Papoulias and T.S. Kosmas, Standard and Non-standard Neutrino-Nucleus Reactions Cross Sections and Event Rates to Neutrino Detection Experiments, Advances in High Energy Physics (2015) Article ID 763648.
- [49] J. Engel, Nuclear form-factors for the scattering of weakly interacting massive particles, Phys. Lett. B (1991) **264**:114–119.

- [50] H.De Vries, C.W. De Jager, and C. De Vries, Nuclear charge-density-distribution parameters from elastic electron scattering, *Atomic Data and Nuclear data tables* (1987) **36**:495–536.
- [51] A. Drukier and L. Stodolsky, Principles and applications of a neutral-current detector for neutrino physics and astronomy, *Phys. Rev. D* (1984) **30**:2295–2309.
- [52] C.J. Horowitz *et al.*, Weak charge form factor and radius of ^{208}Pb through parity violation in electron scattering, *Phys. Rev. C* (2012) **85**:032501–1–5.
- [53] T.S. Kosmas and J.D. Vergados, Nuclear densities with fractional occupation probabilities of the states, *Nucl. Phys. A* (1992) **536**:72–86.
- [54] H.C. Chiang *et al.*, Coherent and incoherent (μ^- , e^-) conversion in nuclei, *Nucl. Phys. A* (1993) **559**:526–542.
- [55] J.N. Bahcall, *Neutrino Astrophysics*, Cambridge University Press, 1989 (Reprint 1990), Melbourne, Australia.
- [56] J. Barranco, O.G. Miranda, T.I. Rashba, Probing new physics with coherent neutrino scattering off nuclei, *Journal of High Energy Physics* (2005) **05**:021.
- [57] J. Barranco, A. Bolanos, O.G. Miranda, and T.I. Rashba, Tensorial NSI and Unparticle physics in neutrino scattering, *Int. J. of Mod. Phys. A* (2012) **27**:1250147.
- [58] J.D. Vergados, F.T. Avignone, and I. Giomataris, Coherent neutral current neutrino-nucleus scattering at a spallation source: A valuable experimental probe, *Phys. Rev. D* (2009) **79**:113001–1–8.
- [59] Y. Giomataris and J.D. Vergados, A network of neutral current spherical TPCs for dedicated supernova detection, *Phys. Lett. B* (2006) **634**:23–29.
- [60] J.D. Vergados and Y. Giomataris, Dedicated supernova detection by a network of neutral current spherical TPC detectors, *Phys. Atom. Nucl.* (2007) **70**:140–149.
- [61] P. Vogel and J. Engel, Neutrino electromagnetic form factors, *Phys. Rev. D* (1989) **39**:3378–3383.
- [62] E. Kolbe, Differential cross sections for neutrino scattering on ^{12}C , *Phys. Rev. C* (1996) **54**:1741–1748.
- [63] K. Langanke and G. Martinez-Pinedo, Nuclear weak-interaction processes in stars, *Rev. Mod. Phys.* (2003) **75**:819–862.
- [64] A. Juodagalvis, K. Langanke, G. Martinez-Pinedo, W.R. Hix, D.J. Dean, and J.M. Sampaio, Neutral-current neutrino-nucleus cross sections for $A \sim 50 - 65$ nuclei, *Nucl. Phys. A* (2005) **747**:87–108.
- [65] K. Langanke, Weak interaction, nuclear physics and supernovae, *Acta Phys. Polon. B* (2008) **39**:265–282.
- [66] W.C. Haxton, Nuclear response of water Cherenkov detectors to supernova and solar neutrinos, *Phys. Rev. D* (1987) **36**:2283–2292.
- [67] T.W. Donnelly and J.D. Walecka, Semi-leptonic weak and electromagnetic interactions in nuclei with application to ^{16}O , *Phys. Lett. B* (1972) **41**:275–280.
- [68] T.W. Donnelly and J.D. Walecka, Elastic magnetic electron scattering and nuclear moments, *Nucl. Phys. A* (1973) **201**:81–106.
- [69] V. Tsakstara and T.S. Kosmas, Nuclear responses of $^{64,66}\text{Zn}$ isotopes to supernova neutrinos, *Phys. Rev. C* (2012) **86**:044618–1–10.
- [70] K.G. Balasi, E. Ydrefors, and T. S. Kosmas, Theoretical study of neutrino scattering off the stable even Mo isotopes at low and intermediate energies, *Nucl. Phys. A* (2011) **868-869**:82–98.
- [71] A.J. Anderson *et al.*, Measuring active-to-sterile neutrino oscillations with neutral current coherent neutrino-nucleus scattering, *Phys. Rev. D* (2012) **86**:013004–1–11.
- [72] A. de Gouvea *et al.*, Working Group Report: Neutrinos (Intensity Frontier Neutrino Working Group), arXiv:1310.4340 [hep-ex] (2013).
- [73] J.N. Bahcall and B.R. Holstein, Solar neutrinos from the decay of 8B , *Phys. Rev. C* (1986) **33**:2121–2127.
- [74] J.N. Bahcall and R.K. Ulrich, Solar models, neutrino experiments, and helioseismology, *Rev. Mod. Phys.* (1988) **60**:297–372.
- [75] J.N. Bahcall *et al.*, Helioseismological Implications of Recent Solar Abundance Determinations, *Astrophys. J.* (2005) **618**:1049–1056.
- [76] W.C. Louis, Searches for muon-to-electron (anti) neutrino flavor change, *Prog. Part. Nucl. Phys.* (2009) **63**:51–73.
- [77] B.R. Davis, P. Vogel, F.M. Mann, and R.E. Schenter, Reactor antineutrino spectra and their application to antineutrino-induced reactions, *Phys. Rev. C* (1979) **19**:2259–2266.
- [78] Y. Declais *et al.*, Study of reactor antineutrino interaction with proton at Bugey nuclear power plant, *Phys. Lett. B* (1994) **338**:383–389.
- [79] O. Tengblad *et al.*, Integral $\bar{\nu}$ -spectra derived from experimental β -spectra of individual fission products, *Nucl. Phys. A* (1989) **503**:136–160.
- [80] S. Kerman *et al.*, Coherency in neutrino-nucleus elastic scattering (TEXONO Collaboration), *Phys. Rev. D* (2016) **93**:113006.
- [81] B. Sevda *et al.*, Constraints on Scalar-Pseudoscalar and Tensorial Non-Standard Interaction and Tensorial Unparticle Couplings from Neutrino-Electron Scattering (TEXONO Collaboration), *Phys. Rev. D* (2017) **95**:033008.
- [82] G. Agnolet *et al.*, Background Studies for the MINER Coherent Neutrino Scattering Reactor Experiment (MINER Collaboration), *Nucl. Instrum. Methods Phys. Res. A* (2017) **853**:53–60.
- [83] H.A. Bethe, Supernova mechanisms, *Rev. Mod. Phys.* (1990) **62**:801–866.
- [84] C. Fröhlich *et al.*, Neutrino-induced nucleosynthesis of $A > 64$ nuclei: the vp process, *Phys. Rev. Lett.* (2006) **96**:142502.
- [85] H.-Th. Janka, and B. Mueller, Neutrino-driven type-II supernova explosions and the role of convection, *Phys. Rep.* (1995) **256**:135–156.
- [86] H.-Th. Janka, K. Langanke, A. Mareka, G. Martinez-Pinedo, and B. Mullera, Theory of core-collapse supernovae, *Phys. Rept.* (2007) **442**:38–74.
- [87] H.T. Janka and W. Hillebrand, Neutrino emission from type II supernovae – an analysis of the spectra, *Astron. Astrophys.* (1989) **224**:49–56.
- [88] M.T. Keil, G.G. Raffelt, and H.-T. Janka, Monte Carlo study of supernova neutrino spectra formation, *Astrophys. J.* (2003) **590**:971–991.
- [89] G.G. Raffelt, M.T. Keil, R. Buras, H.-T. Janka, and M. Rampp, Supernova neutrinos: flavor-dependent fluxes and spectra, *Proc. Neutrino Oscillations and Their Origin* (2004) **03**:380–387.
- [90] H. Duan *et al.*, Stepwise spectral swapping with three neutrino flavors, *Phys. Rev. D* (2008) **77**:085016.
- [91] N. Jachowicz and G.C. McLaughlin, Reconstructing Supernova-Neutrino Spectra using Low-Energy Beta Beams, *Phys. Rev. Lett.* (2006) **96**:172301–1–4.
- [92] V. Tsakstara, T.S. Kosmas, P.C. Divari and J. Sinatkas,

- The interpretation of SN ν signals in terrestrial experiments through the folding procedure, AIP Conf. Proc. (2009) **1180**:140–144.
- [93] V. Tsakstara and T.S. Kosmas, Neutrino-nucleus reactions in terrestrial experiments and astrophysics, Prog. Part. Nucl. Phys. (2010) **64**:407–410.
- [94] K. Scholberg, Supernova signatures of neutrino mass ordering, J.Phys. G (2018) **45**:014002.
- [95] F. Vissani and G. Pagliaroli, The diffuse supernova neutrino background: expectations and uncertainties derived from SN1987A, Astronomy & Astrophysics (2011) **528**:L1.
- [96] K. Moeller, A.M. Suliga, I. Tamborra, P.B. Denton, Measuring the supernova unknowns at the next-generation neutrino telescopes through the diffuse neutrino background, Journal of Cosmology and Astroparticle Physics (2018) **1805**:066.
- [97] A. Bohr and B.R. Mottelson, Nuclear Structure, Benjamin, New York, 1969.